CHINESE OPTICS LETTERS

Vol. 22, No. 3 | March 2024

Nonlinear photonic quasi-periodic spiral

Jing Zeng (曾 静)[1,2], Sen Wang (王 森)[1,2], Ruwei Zhao (赵如薇)[1,2], Yongxing Liu (刘永兴)[1,2], Tiefeng Xu (徐铁峰)[1,2,3], Yan Sheng (盛 艳)[1,2,4*], and Tianxiang Xu (徐天翔)[1,2**]

[1] Laboratory of Infrared Materials and Devices, Research Institute of Advanced Technologies, Ningbo University, Ningbo 315211, China

[2] Zhejiang Key Laboratory of Photoelectric Materials and Devices, Ningbo University, Ningbo 315211, China

[3] Ningbo Institute of Oceanography, Ningbo 315832, China

[4] Department of Quantum Science and Technology, Research School of Physics, Australian National University, Canberra, ACT 2601, Australia

*Corresponding author: shengyan@nbu.edu.cn

**Corresponding author: xutianxiang@nbu.edu.cn

Received September 21, 2023 | Accepted November 9, 2023 | Posted Online March 21, 2024

The design of nonlinear photonic Vogel's spiral based on quasi-crystal theory was demonstrated. Two main parameters of Vogel's spiral were arranged to obtain multi-reciprocal circles. Typical structure was fabricated by the near-infrared femtosecond laser poling technique, forming a nonlinear photonic structure, and multiple ring-like nonlinear Raman–Nath second-harmonic generation processes were realized and analyzed in detail. The structure for the cascaded third-harmonic generation process was predicted. The results could help deepen the understanding of Vogel's spiral and quasi-crystal and pave the way for the combination of quasi-crystal theory with more aperiodic structures.

Keywords: nonlinear photonic quasi-crystal; second-harmonic generation; Vogel's spiral; nonlinear Raman–Nath diffraction; femtosecond laser poling.

DOI: 10.3788/COL202422.031902

1. Introduction

Nonlinear photonic crystals (NPCs) generally refer to materials with periodic second-order nonlinearity $\chi^{(2)}$ and a homogeneous refractive index, and they provide a flexible method to manipulate nonlinear optical parametric processes[1,2]. The famous quasi-phase-matching condition could be satisfied to reach efficient optical frequency conversion and generate entangled photons via spontaneous optical frequency downconversion. Meanwhile, transverse reciprocal lattice vectors may modulate the phase of harmonic waves, achieving nonlinear wavefront shaping[3–9].

Instead of periodic $\chi^{(2)}$ gratings, many NPCs with non-strictly periodic structures, such as Fibonacci and chirped lattices, have been reported widely for broadband or cascaded phase-matching processes[10–12]. These structures can provide multiple components in Fourier space to satisfy several phase-matching conditions at the same time. Among the design method of aperiodic NPC structures, the construction of nonlinear photonic quasi-crystals is an active strategy to obtain the desired reciprocal lattice vectors for the required phase-matching process in any spatial direction[13]. Quasi-crystals are short-range disordered, but long-range ordered structures. In 1984, they were discovered by Shechtman *et al.* in an Al-Mn alloy with extremely rapid cooling, which has a fivefold axis of rotational symmetry, and is not possible in crystallography[14]. In 2005, nonlinear photonic quasi-crystals were first proposed by applying dual-grid quasi-crystal construction[13]. In the past decades, quasi-phase matching with multi-fundamental wavelengths, multi-directions, and other functional nonlinear optical devices based on nonlinear photonic quasi-crystals has been investigated widely[15–24].

Vogel's spiral is a well-known aperiodic structure with a centrosymmetric pattern in Fourier space[25]. The arrangements of seeds in Vogel's spiral could be expressed by the following equations:

$$\begin{cases} r = b\sqrt{n} \\ \theta = n\alpha \end{cases}, \tag{1}$$

where r and θ are the coordinates in the polar coordinate system, b is the parameter describing the density of the seeds, and $n = 0, 1, 2, 3 \ldots$ and α give the azimuthal offset between two adjacent seeds. When α is the golden angle $[\varphi = (1 + \sqrt{5})/2, \alpha = 2\pi/\varphi^2 \approx 2.4]$, the structure evolves into the famous sunflower lattice, also called a golden-angle spiral, exhibiting an inner sharp ring with outer weak rings in the Fourier spatial spectrum[26]. On the basis of this unique property, the sunflower-structured photonic crystals, photonic crystal fibers, and nanoparticles have shown

characteristic performances in complete photonic bandgap, birefringence, optical orbital angular momentum control, wave focusing, and mode localization[27–31]. In nonlinear optics, the sharp ring-like peak in the Fourier spectrum means a possibly efficient phase-matching process. Thus, the golden-angle spiral-structured NPCs were proven to have a prominent effect on the enhancement of broadband Čerenkov second-harmonic generation[32]. This is the sole application example of Vogel's spiral in nonlinear optics with the generation of an annular second-harmonic signal. However, its application in multichannel second-harmonic wave production is unknown, so the application of Vogel's spiral-structured NPCs in other fields, such as generation of entangled photon pairs and quantum communication, is restricted.

In this paper, the quasi-crystal theory and Vogel's spiral were combined to obtain structures with strong multirings in the Fourier spatial spectrum. A typical spiral was fabricated by near-infrared femtosecond laser poling, forming nonlinear photonic quasi-periodic spirals, and second-harmonic generation via nonlinear Raman–Nath diffraction was captured and discussed. Furthermore, a nonlinear photonic quasi-periodic spiral aiming at cascaded third-harmonic generation was designed. This work may provide new ideas for the design of hybrid nonlinear photonic structures.

2. Structure Design and Fabrication

In accordance with the Vogel's spiral expressed by Eq. (1), as a universal rule, when α is an irrational, the spiral is approximately homogeneous and isotropic. Hence, diffuse rings constitute the Fourier spectrum, with the innermost one being far stronger than the outer ones. When the isotropy is destroyed, e.g., when α is a rational number, radial arms form in Vogel's spiral, and the Fourier spectrum shows several scattered rings instead of a single strong ring[33]. The isotropy of the golden-angle spiral must be destroyed on purpose to obtain a spiral with two or more desired sharp rings near the center in the Fourier spectrum. For this aim, the concept of the quasi-crystal could be borrowed.

Figure 1(a) shows an example of a golden-angle spiral. The radius of the sharp ring in Fourier space [Fig. 1(d)] relates to the distance between two adjacent seeds. This distance is nearly equal in the golden-angle spiral and determined by the parameter b in Eq. (1). Here, if α or b is no longer a constant, but an arrangement of two numbers instead, the distance could vary drastically from each seed pair to another, and the ring in Fourier space could split.

The cut-and-project method for quasi-crystal construction is employed[34]. First, the quasi-crystal is constructed by two angles, with α_1 being the golden angle and $\alpha_2 = 1.57$. A series of quasi-periodic angles with approximate radian values of 0, 1.57, 3.97, 6.37 ... could be obtained. In the new spiral, the $(q+1)$th value from the smallest to the largest is set as $\theta(q+1)$ with $q = 0, 1, 2, 3 \ldots$. The spiral function is as follows:

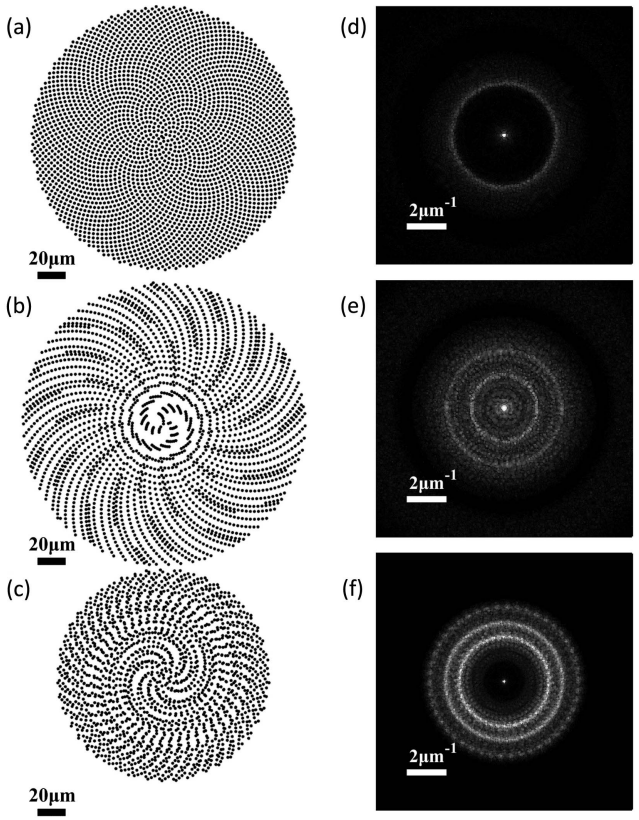

Fig. 1. (a) Golden-angle spiral with $b = 1.70$ μm and a total of 3000 points; (b) nonlinear photonic quasi-periodic spiral structure based on rearrangement of α, with the two construction parameters α_1 being the golden angle and $\alpha_2 = 1.57$, $b = 1.70$ μm; (c) nonlinear photonic quasi-periodic spiral structure based on rearrangement of b, with the two construction parameters $b_1 = 1.50$ μm and $b_2 = 2.00$ μm; (d)–(f) Fourier spatial spectra of (a)–(c).

$$\begin{cases} r = b\sqrt{q} \\ \theta = \theta(q+1) \end{cases}, \tag{2}$$

where α_1 and α_2 are the construction parameters for $\theta(q+1)$. The quasi-periodic spiral expressed by Eq. (2) with $b = 1.70$ μm is shown by Fig. 1(b). This spiral has two elements: a golden-angle spiral with $b = 1.70$ μm [Fig. 2(a)] and Vogel's spiral with $\alpha = \alpha_2$ and $b = 1.70$ μm [Fig. 2(b)]. The distance between the adjacent seeds in Fig. 1(b) is no longer invariable. The Fourier spectrum of Fig. 1(b) is shown in Fig. 1(e). Two sharp rings near the central region emerge. Then, the quasi-crystal constructed by two distances was considered as follows: $b_1 = 1.50$ μm and $b_2 = 2.00$ μm. Similar to that constructed by two angles, quasi-period-arranged distance values could be provided by the cut-and-project method, and the $(q+1)$th value from the smallest to the largest is set as $b(q+1)$ with $q = 0, 1, 2, 3 \ldots$. The spiral function is as follows:

$$\begin{cases} r = b(q+1) \\ \theta = q\alpha \end{cases}, \tag{3}$$

where b_1 and b_2 are the construction parameters for $b(q+1)$. The typical spiral pattern with α being the golden-angle spiral is shown in Fig. 1(c), and its two elements are exhibited by Fig. 2(c) (golden-angle spiral, $b = b_1$) and Fig. 2(d) (golden-angle spiral, $b = b_2$). The corresponding Fourier spatial spectrum of Fig. 1(c) is exhibited in Fig. 1(f). Two sharp rings can be found, with another external one with weaker strength. These results indicate that the nonuniformity of α and b could be utilized for multiring-like peaks in Fourier space.

For nonlinear photonic quasi-periodic spirals, the radius of rings in the Fourier spatial spectrum indicates the magnitude of the reciprocal lattice vector, which is pivotal in quasi-phase matching. So, a definite relationship between the ring radius and elements of the quasi-periodic spiral is essential. As shown in the quasi-periodic spiral in Fig. 1(b), the radii of the two rings in its Fourier spectrum [Fig. 1(e)] were calculated to be 1.29 and 2.21 μm^{-1}. The Fourier spectra in Figs. 2(a) and 2(b) are shown by Figs. 2(e) and 2(f). In Fig. 2(e), a sharp ring with a radius of 2.04 μm^{-1} emerges, which is separated from the two in Fig. 1(e). As shown in Fig. 2(f), no available ring-like reciprocal lattice vectors are present due to the formation of radial arms in Fig. 2(b). The quasi-periodic spiral expressed by Eq. (2) with different construction parameters was studied, and the ring radius in Fourier spatial spectrum can be hardly predicted. In other words, the numerical relationship between the radius of the two rings in Fig. 1(e) with α_1 and α_2 is uncertain, which is not friendly for the design of the desired centrosymmetric ring-like reciprocal lattice vectors by a quasi-periodic spiral following Eq. (2).

Two elements of the quasi-periodic spiral shown in Fig. 1(c) are demonstrated by Figs. 2(c) and 2(d), with Figs. 2(g) and 2(h) exhibiting their Fourier spectra. On the basis of the basic characteristic of being a golden-angle spiral, a sharp ring near the center is located in both of the two patterns. Their radii were calculated to be 1.75 [Fig. 2(g)] and 2.28 μm^{-1} [Fig. 2(h)]. In Fig. 1(c), the rearranged b_1 and b_2 do not break the isotropy of the spiral but only change the average distance of the adjacent seeds from one constant to two constants. So, the radii of the innermost and middle rings in Fig. 1(f) were calculated to be the same as the ones shown in Figs. 2(f) and 2(h). In other words, as long as two golden-angle spirals with ring-like reciprocal lattice vector of given magnitude are designed, the quasi-periodic spiral simultaneously providing the two annular vectors could be obtained by the combination of the two golden-angle spirals following Eq. (3). For deep understanding of this method, the relation between the radius of the ring in the Fourier spectrum with b in Eq. (1) can be considered. In a golden-angle spiral, the radius of the ring is inversely proportional to the average particle spacing of the structure, which is determined by b[33]. When b is a quasi-periodic arrangement of b_1 and b_2 [Fig. 1(c)], its manifestation in the Fourier spatial spectrum [Fig. 1(f)] should correspond with spirals with the two parameters severally. In addition to the two inner rings, a new ring is present, with the radius of 2.90 μm^{-1}. This ring comes from the increased disorder, similar to the rings in Fig. 1(e) by rearrangement of α. The magnitude of this new ring is also unpredictable.

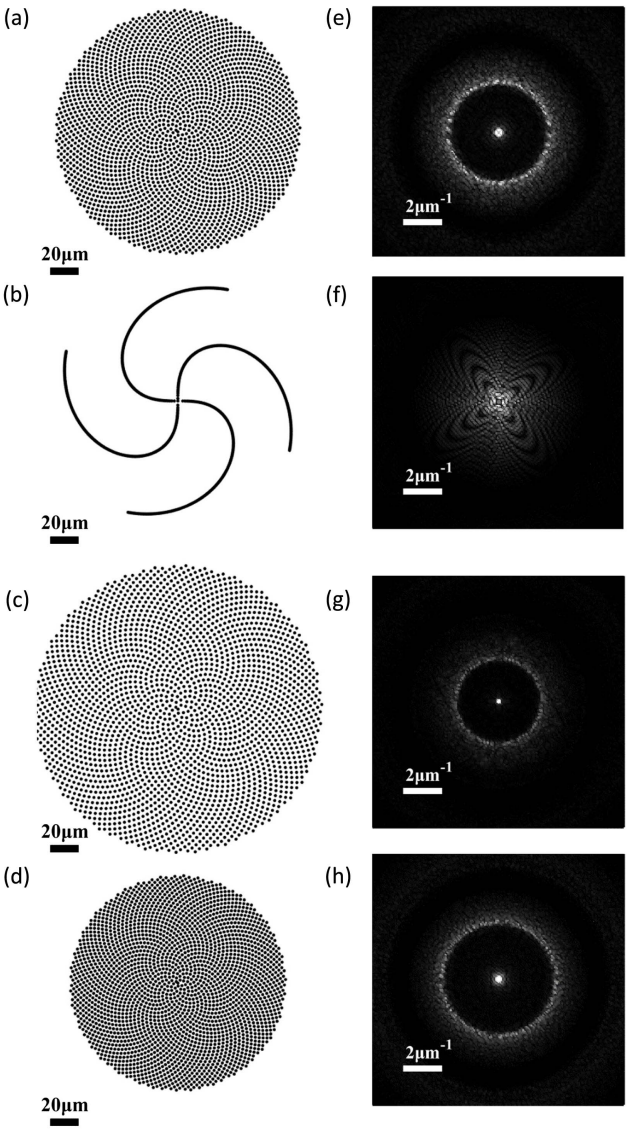

Fig. 2. (a) Golden-angle spiral with $b = 1.70$ μm [an element of quasi-periodic spiral shown in Fig. 1(b)]; (b) Vogel's spiral with $\alpha = 1.57$ and $b = 1.70$ μm [the other element of quasi-periodic spiral shown in Fig. 1(b)]; (c) golden-angle spiral with $b = 1.50$ μm [an element of quasi-periodic spiral shown in Fig. 1(c)]; (d) golden-angle spiral with $b = 2.00$ μm [the other element of quasi-periodic spiral shown in Fig. 1(c)]; (e)–(h) Fourier spatial spectra of (a)–(d).

The spiral shown in Fig. 1(c) was employed for experimental investigation. The structure was machined out in an x-cut strontium barium niobate ferroelectric crystal ($Sr_{0.61}Ba_{0.39}NbO_3$, SBN) by using infrared femtosecond laser poling at room temperature[35]. The size of the crystal is 5 mm × 5 mm × 1 mm, with the x-surfaces being polished for femtosecond laser processing and nonlinear detection. The SBN crystal was mounted on a translatable stage that can be moved along the x, y, and z directions with a resolution of ~100 nm. The laser used in processing of this structure is a Ti:sapphire laser system (Chameleon Ultra II, Coherent) operated at 750 nm with a pulse width of 141 fs and a repetition frequency of 80 MHz.

The processing light polarized along the z axis of the crystal was focused by an objective lens (50×, NA = 0.65) with a beam diameter of 1.2 ± 0.2 mm and was incident normally into the crystal cross the x-surface. This laser focus was about 90 μm below the x-surface of the crystal. A halogen lamp was used to illuminate the crystal. When processing the structure, the laser power was regulated using a half-wave plate and a polarizer, and the working pulse energy was regulated to 1.5–4 nJ during processing. The laser was chopped using an automatic shutter (SH05, Thorlabs). Each point was flashed 2 times with the laser to obtain domain inversion effectively[36].

3. Results and Discussion

Second-harmonic generation based on the fabricated nonlinear photonic quasi-periodic spiral was carried out with a broadband femtosecond laser source (Chameleon Compact OPO, 1000–1600 nm) as the fundamental light. The beam was focused by a 10× microscopic objective (NA = 0.3) and was incident perpendicular to the crystal surface. The generated second-harmonic signal was projected onto the light screen at far field, and then the diffraction pattern of the second-harmonic wave was photographed using a charge-coupled device (CCD) camera. Different wavelengths (1480–1580 nm) were used for the observation of the structure. The diffraction patterns produced using different wavelengths were similar. Typical patterns obtained with the fundamental wavelengths at 1480 nm are shown by Fig. 3(a), with three distinct rings present in this image. The color in this figure is artificial for enhanced visualization.

The three ring-like second-harmonic waves are produced by nonlinear Raman–Nath diffraction[37]. The phase-matching condition could be expressed as follows:

$$\boldsymbol{k}_2 \sin\theta_m - \boldsymbol{G}_m = 0. \tag{4}$$

The geometrical diagram is exhibited in Fig. 3(b), where $\boldsymbol{k}_1$ and $\boldsymbol{k}_2$ represent the wave vectors of the fundamental and second-harmonic waves; $\boldsymbol{G}_m$ is the reciprocal lattice vector; θ_m is the corresponding internal divergence angle of $\boldsymbol{k}_2$ relative to $\boldsymbol{k}_1$; $\Delta\boldsymbol{k}_m$ is the longitudinal phase mismatch; and $m = 1, 2$, and 3 denote the innermost, middle, and outermost ring, respectively. The three reciprocal lattice vectors provided by the processed structure are $G_1 = 1.75\,\mu\text{m}^{-1}$, $G_2 = 2.28\,\mu\text{m}^{-1}$, and $G_3 = 2.90\,\mu\text{m}^{-1}$. The longitudinal phase mismatches of the three ring-like second-harmonic waves are $\Delta k_1 = 0.37\,\mu\text{m}^{-1}$, $\Delta k_2 = 0.31\,\mu\text{m}^{-1}$, and $\Delta k_3 = 0.23\,\mu\text{m}^{-1}$. The proportion of vectors in Fig. 3(b) was exaggerated for enhanced visualization. External divergence angles β_m could be obtained by the internal angles θ_m, Snell's law, and the Sellmeier equation of SBN crystal[38]. The measured results are shown in Table 1. They fit well with the calculated angles. In the as-grown x-cut SBN crystal, spontaneous domains along the z direction providing random reciprocal lattice vectors in the x–y plane can be obtained. They can produce random quasi-phase-matched second-harmonic generation. The transverse bright streaks in Fig. 3(a) are second-harmonic signals modulated by the spontaneous domains[39]. The theoretical external angles of the

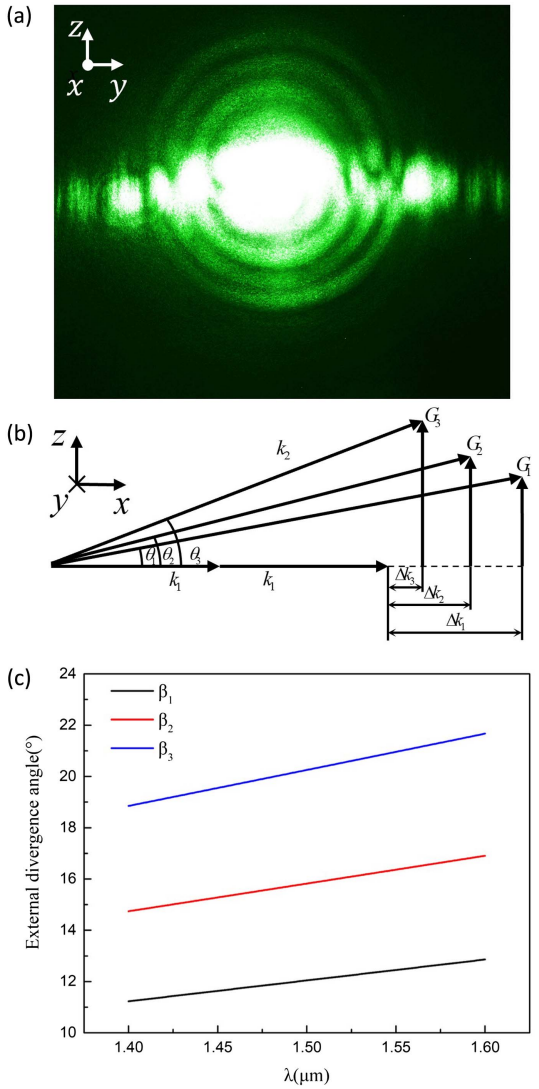

Fig. 3. (a) Typical second-harmonic pattern generated by the fabricated nonlinear photonic quasi-periodic spiral. Three ring-like patterns are modulated by the designed structure via nonlinear Raman–Nath diffraction. The crosswise line that lies in the middle is produced by spontaneous domains. (b) Geometrical relation of the phase-matching condition of nonlinear Raman–Nath diffraction; (c) variation tendency of external angle relying on fundamental wavelength.

Table 1. Theoretical and Experimental Values of External Nonlinear Raman–Nath Diffraction Angles with λ = 1480 nm.

	β_1	β_2	β_3
Theoretical angle (°)	11.89	15.89	19.79
Experimental angle (°)	11.55	15.54	19.61

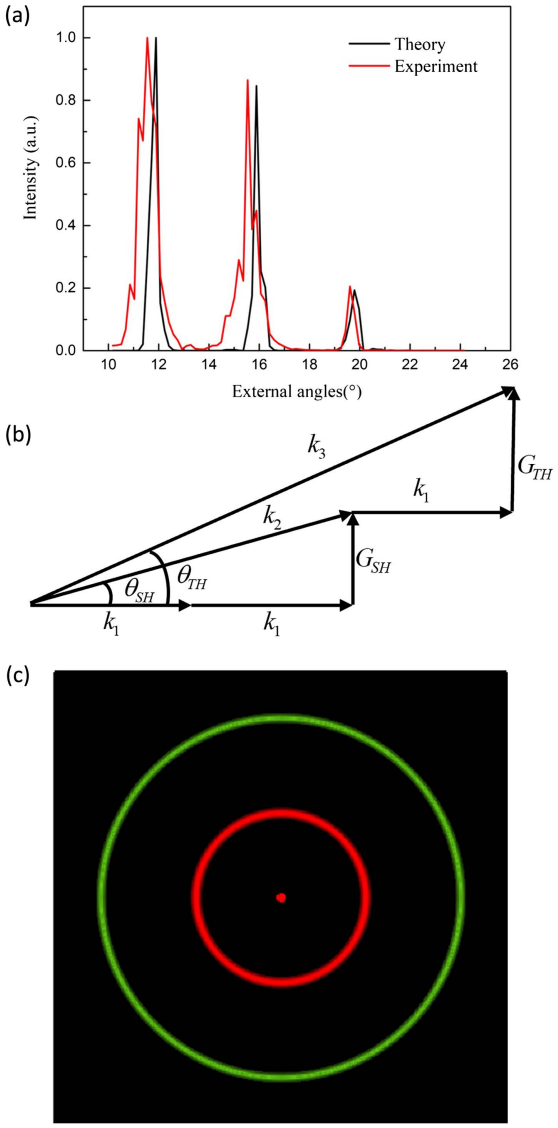

Fig. 4. (a) Experimental and theoretical curves of second-harmonic intensity depending on external diffraction angle; (b) phase-matching diagram of third-harmonic generation in desired nonlinear photonic quasi-periodic spiral; (c) calculated pattern of cascaded third-harmonic and second-harmonic waves.

second-harmonic rings that depend on the fundamental wavelength are shown in Fig. 3(c). As a phase mismatch exists in nonlinear Raman–Nath diffraction, the external angles change slowly with the variation of wavelength.

The relative intensities of the three rings in Fig. 3(a) are shown by the red line in Fig. 4(a). The intensities of second-harmonic waves produced by nonlinear Raman–Nath diffraction can be simulated by considering phase mismatch and Fourier components following the equation

$$I_2 \propto c_m^2 \,\mathrm{sinc}^2\left(\frac{\Delta k_m}{2}\right), \tag{5}$$

where I_2 is the intensity of the second-harmonic beam, and c_m is the Fourier coefficient. The modulation by random reciprocal lattice vectors is ignored in calculation. The theoretical second-harmonic intensities related to the external diffraction angles are shown by the black curve in Fig. 4(a), which fits well with the experimental results. The slight errors may be caused by the Sellmeier equation and the component of the SBN crystal, as the refractive indices relate closely with the ratio of Sr and Ba in SBN.

The demonstrated nonlinear photonic quasi-periodic spiral by Eq. (3) has an extensive effect in complicated optical frequency conversion processes such as cascaded third-harmonic generation and spontaneous frequency downconversion. With third-harmonic generation as an example, appropriate ring-like reciprocal lattice vectors could realize frequency doubling and sum frequency generation processes simultaneously. The fundamental wavelength is assumed to be 1560 nm and perpendicular to the spiral, and the spiral was fabricated in the x-cut SBN crystal. Nonlinear Bragg diffraction should be realized without phase mismatch to obtain a fine conversion efficiency. The phase-matching diagram is shown in Fig. 4(b) on the basis of a phase-matching condition as follows:

$$\begin{cases} 2\boldsymbol{k}_1 + \boldsymbol{G}_{\mathrm{SH}} = \boldsymbol{k}_2 \\ \boldsymbol{k}_2 + \boldsymbol{k}_1 + \boldsymbol{G}_{\mathrm{TH}} = \boldsymbol{k}_3 \end{cases}, \tag{6}$$

where $\boldsymbol{k}_1, \boldsymbol{k}_2$, and $\boldsymbol{k}_3$ are the wave vectors of the fundamental, second-harmonic, and third-harmonic waves, respectively, and $\boldsymbol{G}_{\mathrm{SH}}$ and $\boldsymbol{G}_{\mathrm{TH}}$ are the transverse reciprocal lattice vectors for second- and third-harmonic generation, respectively. In Fig. 4(b), θ_{SH} and θ_{TH} are internal divergence angles of $\boldsymbol{k}_2$ and $\boldsymbol{k}_3$ relative with $\boldsymbol{k}_1$. Taking fundamental wavelength and Sellmeier equation of SBN into consideration, G_{SH} and G_{TH} should be 3.76 and 7.96 $\mu\mathrm{m}^{-1}$, respectively, and θ_{SH} and θ_{TH} should be 11.95° and 16.43°, respectively, with the corresponding external angles being 27.79° and 41.23°, respectively, to achieve the geometrical relation in Eq. (6).

The two parameters were calculated to be $b_1 = 0.93$ and $b_2 = 0.44\,\mu\mathrm{m}$ for the construction of the quasi-periodic spiral by Eq. (3) to proceed with the third-harmonic generation via nonlinear Bragg diffraction on the basis of Eq. (6). In the spiral shown by Fig. 1(c), the closest distance between two seeds is 1.15 μm, which almost reached the size limitation in femtosecond laser-induced domain inversion. The closest distance between two seeds in the spiral for third-harmonic generation is 0.30 μm, which is difficult to fabricate. So, the third-harmonic generation process was exhibited in theory, and the calculated pattern containing the inside second-harmonic ring and the outside third-harmonic ring is shown in Fig. 4(c). In fact, an outermost ring is still present in the Fourier spatial spectrum of the designed spiral for third-harmonic generation with the radius of 12.16 $\mu\mathrm{m}^{-1}$. When the fundamental wavelength is 1560 nm, this ring may also modulate harmonic waves via nonlinear Raman–Nath diffraction with the existence of the phase mismatch. However, the efficiency should be far below the third-harmonic generation via nonlinear Bragg diffraction. So, the effect of the outermost ring is ignored in Fig. 4(c). Furthermore, if other wavelength components could be added in the incident

fundamental wave, an additional phase-matching condition could be satisfied. For example, by utilizing the collinear second-harmonic wave, which is modulated by the random domains such as the central bright spot in Fig. 3(b), the outermost ring could generate another third-harmonic wave when a light source of 1372 nm is coupled into the incident beam.

4. Conclusion

In summary, a nonlinear photonic quasi-periodic spiral was designed based on the basis of the combination of Vogel's spiral and quasi-crystal theory. Two basic parameters of Vogel's spiral, α and b, were rearranged to form a quasi-periodic spiral, which can provide multiple ring-like peaks in the Fourier spatial spectrum. The predictability of the ring radius was discussed, and the quasi-periodic spiral constructed by the rearrangement of b was employed for further study. A typical structure was fabricated by femtosecond laser-induced domain inversion in a ferroelectric SBN crystal to produce a nonlinear photonic quasi-periodic spiral. Conical second-harmonic generation via nonlinear Raman–Nath diffraction was captured. The characteristics of the second-harmonic patterns were measured, and they fit well with the theoretical prediction. The nonlinear photonic quasi-periodic spiral for cascaded third-harmonic generation was investigated in theory. The results may help with the extension of quasi-periodic theory and pave the way for the design of hybrid nonlinear photonic quasi-periodic spirals.

Acknowledgements

This work was supported by the National Natural Science Foundation of China (Nos. 62275136, 61905124, 12274248, and 62090063), the Natural Science Foundation of Zhejiang Province (No. LY22F050009), the Yongjiang Scholar Foundation of Ningbo, and the K. C. Wong Magna Fund of Ningbo University.

References

1. V. Berger, "Nonlinear photonic crystals," Phys. Rev. Lett. **81**, 4136 (1998).
2. J. A. Armstrong, N. Blgemeergen, J. Ducuing, *et al.*, "Interactions between light waves in a nonlinear dielectric," Phys. Rev. **127**, 1918 (1962).
3. X. Yu, P. Xu, Z. Xie, *et al.*, "Transforming spatial entanglement using a domain-engineering technique," Phys. Rev. Lett. **101**, 233601 (2008).
4. T. Ellenbogen, N. Voloch, A. Ganany-Padowicz, *et al.*, "Nonlinear generation and manipulation of Airy beams," Nat. Photonics **3**, 395 (2009).
5. H. Jin, P. Xu, X. Luo, *et al.*, "Compact engineering of path-entangled sources from a monolithic quadratic nonlinear photonic crystal," Phys. Rev. Lett. **111**, 023603 (2013).
6. E. Megidish, A. Halevy, H. Eisenberg, *et al.*, "Compact 2D nonlinear photonic crystal source of beamlike path entangled photons," Opt. Express **21**, 6689 (2013).
7. X. H. Hong, B. Yang, C. Zhang, *et al.*, "Nonlinear volume holography for wave-front engineering," Phys. Rev. Lett. **113**, 163902 (2014).
8. S. Trajtenberg-Mills, I. Juwiler, and A. Arie, "On-axis shaping of second-harmonic beams," Laser Photonics Rev. **9**, L40 (2015).
9. X. Hu, Y. Zhang, and S. Zhu, "Nonlinear beam shaping in domain engineered ferroelectric crystals," Adv. Mater. **32**, 1903775 (2020).
10. S. N. Zhu, Y. Y. Zhu, and N. B. Ming, "Quasi-phase-matched third-harmonic generation in a quasi-periodic optical superlattice," Science **278**, 843 (1997).
11. Y. Q. Qin, C. Zhang, Y. Y. Zhu, *et al.*, "Wave-front engineering by Huygens-Fresnel principle for nonlinear optical interactions in domain engineered structures," Phys. Rev. Lett. **100**, 063902 (2008).
12. T. Ellenbogen, A. Ganany-Padowicz, and A. Arie, "Nonlinear photonic structures for all-optical deflection," Opt. Express **16**, 3077 (2008).
13. R. Lifshitz, A. Arie, and A. Bahabad, "Photonic quasicrystals for general purpose nonlinear optical frequency conversion," Phys. Rev. Lett. **95**, 133901 (2005).
14. D. Shechtman, R. J. Schaefer, and F. Biancaniello, "Precipitation in rapidly solidified Al-Mn alloys," Metall. Trans. A **15**, 1987 (1984).
15. B. Freedman, G. Bartal, M. Segev, *et al.*, "Wave and defect dynamics in nonlinear photonic quasicrystals," Nature **440**, 1166 (2006).
16. A. Ganany-Padowicz, I. Juwiler, O. Gayer, *et al.*, "Engineering two-dimensional nonlinear photonic quasi-crystals," Opt. Lett. **33**, 1386 (2008).
17. A. Bahabad, R. Lifshitz, N. Voloch, *et al.*, "Nonlinear photonic quasicrystals for novel optical devices," Philos. Mag. **88**, 2285 (2008).
18. Y. Sheng, K. Koynov, J. Dou, *et al.*, "Collinear second harmonic generations in a nonlinear photonic quasicrystal," Appl. Phys. Lett. **92**, 201113 (2008).
19. A. Ganany-Padowicz, I. Juwiler, O. Gayer, *et al.*, "All-optical polarization switch in a quadratic nonlinear photonic quasicrystal," Appl. Phys. Lett. **94**, 091108 (2009).
20. A. Arie and N. Voloch, "Periodic, quasi-periodic, and random quadratic nonlinear photonic crystals," Laser Photonics Rev. **4**, 355 (2010).
21. S. F. Liew, H. Noh, J. Trevino, *et al.*, "Localized photonic band edge modes and orbital angular momenta of light in a golden-angle spiral," Opt. Express **19**, 23631 (2011).
22. L. Zhao, Z. Qi, Y. Yuan, *et al.*, "Integrated noncollinear red–green–blue laser light source using a two-dimensional nonlinear photonic quasicrystal," J. Opt. Soc. Am. B **28**, 608 (2011).
23. L. Zhao, J. Liu, Y. Gao, *et al.*, "Nonlinear optical properties of a two-dimensional nonlinear photonic quasicrystal based on second order cascaded nonlinearities," J. Mod. Opt. **63**, 239 (2016).
24. J. Trevino, H. Cao, and L. Dal Negro, "Circularly symmetric light scattering from nanoplasmonic spirals," Nano Lett. **11**, 2008 (2011).
25. S. F. Liew, *Light Transport and Lasing in Complex Photonic Structures* (Yale University, 2014).
26. H. Vogel, "A better way to construct the sunflower head," Math. Biosci. **44**, 179 (1979).
27. D. Chang, J. Scheuer, and A. Yariv, "Optimization of circular photonic crystal cavities - beyond coupled mode theory," Opt. Express **13**, 9272 (2005).
28. N. Lawrence, J. Trevino, and L. Dal Negro, "Control of optical orbital angular momentum by Vogel spiral arrays of metallic nanoparticles," Opt. Lett. **37**, 5076 (2012).
29. T. Zhao, Y. Hu, S. Fu, *et al.*, "Aperiodic Vogel spirals for broadband optical wave focusing," Opt. Lett. **43**, 5969 (2018).
30. F. Sgrignuoli, R. Wang, F. Pinheiro, *et al.*, "Localization of scattering resonances in aperiodic Vogel spirals," Phys. Rev. B **99**, 104202 (2019).
31. M. Aeschlimann, T. Brixner, F. Fenner, *et al.*, "Direct imaging of photonic band-edge states in golden Vogel spirals using photoemission electron microscopy," J. Opt. Soc. Am. B **40**, B19 (2023).
32. S. Liu, K. Switkowski, X. Chen, *et al.*, "Broadband enhancement of Čerenkov second harmonic generation in a sunflower spiral nonlinear photonic crystal," Opt. Express **26**, 8628 (2018).
33. J. Trevino, S. F. Liew, H. Noh, *et al.*, "Geometrical structure, multifractal spectra and localized optical modes of aperiodic Vogel spirals," Opt. Express **20**, 3015 (2012).
34. M. Senechal, *Quasicrystals and Geometry* (Cambridge University, 1995).
35. T. Xu, K. Switkowski, X. Chen, *et al.*, "Three-dimensional nonlinear photonic crystal in ferroelectric barium calcium titanate," Nat. Photonics **12**, 591 (2018).
36. S. Wang, S. Liu, D. Liu, *et al.*, "Ferroelectric domain engineering with femtosecond pulses of different wavelengths," Opt. Express **31**, 5843 (2023).
37. Y. Sheng, Q. Kong, W. Wang, *et al.*, "Theoretical investigations of nonlinear Raman–Nath diffraction in the frequency doubling process," J. Phys. B At. Mol. Opt. Phys. **45**, 055401 (2012).
38. T. Woike, T. Granzow, U. Dörfler, *et al.*, "Refractive indices of congruently melting $Sr_{0.61}Ba_{0.39}Nb_2O_6$," Phys. Status Solidi **186**, R13 (2001).
39. P. Molina, M. de la O. Ramírez, and L. E. Bausá, "Strontium barium niobate as a multifunctional two-dimensional nonlinear 'photonic glass'," Adv. Func. Mater. **18**, 709 (2008).